MATHEMATICAL MODELING OF MICROTUBULE DYNAMIC INSTABILITY: NEW INSIGHT INTO THE LINK BETWEEN GTP-HYDROLYSIS AND MICROTUBULE AGING *

Ayuna Barlukova[1], Diana White[2], Gérard Henry[1], Stéphane Honoré[3] and Florence Hubert[1,*]

Abstract. Microtubules (MTs) are protein polymers that exhibit a unique type of behavior referred to as dynamic instability. That is, they undergo periods of growth (through the addition of GTP-tubulin) and shortening (through the subtraction of GDP-tubulin). Shortening events are very fast, where this transition is referred to as a catastrophe. There are many processes that regulate MT dynamic instability, however, recent experiments show that MT dynamics may be highly regulated by a MTs age, where young MTs are less likely to undergo shortening events than older ones. In this paper, we develop a novel modeling approach to describe how the age of a MT affects its dynamic properties. In particular, we extend on a previously developed model that describes MT dynamics, by proposing a new concept for GTP-tubulin hydrolysis (the process by which newly incorporated GTP-tubulin is hydrolyzed to lower energy GDP-tubulin). In particular, we assume that hydrolysis is mainly vectorial, age-dependent and delayed according to the GTP-tubulin incorporation into the MT. Through numerical simulation, we are able to show how MT age affects certain properties that define MT dynamics. For example, simulations illustrate how the aging process leads to an increase in the rate of GTP-tubulin hydrolysis for older MTs, as well as increases in catastrophe frequency. Also, since it has been found that MT dynamic instability is affected by chemotherapy microtubule-targeting agents (MTAs), we highlight the fact that our model can be used to investigate the action of MTAs on MT dynamics by varying certain model parameters.

Mathematics Subject Classification. 92C50, 35Q80, 74S10.

Received September 17, 2016. Accepted April 26, 2017.

1. Introduction

Microtubules (MTs) are rigid protein polymers that self-assemble from α-β- tubulin heterodimers, helping to form the cytoskeleton of all eukaryotic cells [24]. MTs are crucial to normal cell development, playing important

[1] Aix Marseille University, CNRS, Centrale Marseille, Institut de Mathématiques de Marseille, Marseille, France.

[2] Clarkson University, Department of Mathematics, Potsdam, New York, USA.

[3] Aix-Marseille University, INSERM, Center of Research in Oncobiology and Oncopharmacology, Marseille, France.

*Corresponding author: `florence.hubert@univ-amu.fr`

roles in many cellular processes. Such processes include the regulation of substrate adhesion and cell polarity during cell migration, and the segregation of chromosomes during cell division. Because of their role in cell migration and cell division, MTs are a key contributor to cancer progression. As such, they are frequently used as targets for many microtubule targeting agents (MTAs) used in cancer treatments.

MTs display a unique type of dynamical behavior, undergoing transitions between sustained periods of growth and rapid shortening. This phenomenon is referred to as MT dynamic instability, and was first observed by Mitchison and Kirschner in 1984 [29]. MTs have a polar structure, where the "-end" of a MT has the majority of α-tubulin exposed and the "+end" of a MT has the majority of β-tubulin exposed. Dynamic instability is observed *in vitro* with pure tubulin at both ends of the MT, suggesting that it is an intrinsic property of MTs. It is also observed in cells, where it is regulated by many associated proteins at both ends of a MT [9,19,29].

Although MTs can be dynamic at both ends *in vitro*, we generally only consider modeling the +end dynamics, since variations at this end are much faster and larger than those at the -end. Moreover, *in vivo*, MT -ends are often capped (by capping proteins) or anchored at the nucleation site (which is referred to as the MT Organizing Center), and so they are not always dynamic.

A MT polymerizes by the addition of free guanosine triphosphate (GTP)-tubulin heterodimers at its +end. As GTP-tubulin is added to a MT, it is hydrolyzed (at some rate) to lower energy guanosine diphosphate (GDP)-tubulin. In general, the majority of a MT is composed of GDP-tubulin, where only several layers of GTP-tubulin exist at the growing +end. This small GTP region is referred to as the "GTP-cap". The GTP-cap has long been postulated to exist, but it is only recently that experiments have provided quantitative measurements of its structure. This has been made possible by the discovery that end-binding proteins (EBs) have the ability to bind to the GTP-cap by sensing the nucleotide state of tubulin at this location [1,5,27,35].

If a MT polymerizes at a rate larger than that of hydrolysis, the MT will continue to grow. However, if the rate of hydrolysis is larger than the growth rate, the GTP-cap shortens. When the GTP-cap disappears the MT depolymerizes very quickly. The transition to a state of depolymerization is called a catastrophe event. As a MT shortens, it's possible that is can transition back into a state of polymerization, before depolymerizing completely. Such an event is called a rescue.

Over the past few decades, many stochastic and deterministic models for MT dynamic instability have been proposed [2,6,7,11,12,16,17,20,22,26,32,33,36]. Stochastic models are used to describe MT dynamics at the microscopic level, taking into consideration the addition and subtraction of individual tubulin dimers [7], while deterministic models describe dynamics at a macroscopic level. Examples of such macroscopic models include systems of differential equations that describe the time evolution of the length distributions for growing and shortening MT populations [11,17].

The first stochastic description for MT dynamic instability was developed by Hill and Chen in 1984 [7]. Hill and Chen used Monte Carlo kinetic simulations to describe dynamic instability at the extreme tip of a MT. They called their model the "cap" model – the word "cap" comes from the resulting behavior found from simulations. In particular, they found that below a critical concentration for tubulin, MTs exist in either one of two phases: capped (by GTP) or uncapped (with no GTP). In the capped phase, the MT grows (with a fluctuating size in cap), and in the uncapped phase the MT quickly depolymerizes. Although this model is useful at capturing the qualitative description of MT dynamic instability found in experiment, it does not give a wholly accurate quantitative description. From their simulations, Hill and Chen found a critical concentration which is about one seventh of the experimental critical concentration determined by Mitchinson and Kirschner [29].

One of the first deterministic models describing MT dynamic instability was proposed by Dogterom and Leibler in 1993 [11]. The model consists of a pair of partial differential equations (PDEs), used to describe the time evolution of the length distributions for growing and shortening MTs. MT growth and shortening is described as an advection process, where the rates of both growth and shortening are constant. Further, MTs switch between growing a shortening states, where the switching rates correspond to the rescue and catastrophe frequencies. This approach is a good first approximation, and has been successfully used to qualitatively describe MT behavior at the population level. In particular, this model has been used to accurately describe the exponentially distributed array of MTs found centered at the centrosome in interphase cells [11]. One limitation

of this model is that catastrophe and rescue frequencies are inputs to the model. The frequencies for which MTs undergo catastrophe and rescue are quantities that help define the dynamic properties of MTs *in vivo* and *in vitro* [37]. In this paper, we come up with mathematical descriptions for such quantities, and use these quantities to compare simulation results with experiment.

A recent model for MT dynamic instability by Hinow *et al.* [17] describes MT growth and shortening using a similar advection process as Dogterom and Leibler [11]. However, unlike the approach used in [11], Hinow *et al.* suppose that the growth rate is dependent on the free tubulin concentration, a phenomenon that has been observed in experiments [24]. The latter experiments have shown that when the free tubulin concentration is low, MTs do not grow; at a lower threshold tubulin concentration, MTs grow at a rate that depends linearly on the free tubulin concentration; finally, past an upper threshold for tubulin concentration, the MT growth rate is constant [24]. In accordance with experiment, the model of Hinow *et al.* assumes that MT growth rates increase linearly with increasing tubulin concentration. However, this model does not include critical tubulin concentration thresholds under which MTs do not grow, and above which the MT growth rate saturates and is thereafter independent of tubulin concentration.

Results from recent studies suggest that catastrophe events depend on MT "aging". In [8, 14, 21, 30, 38], MT aging is described as a multistep process caused by successive defects that propagate along a MT tip. From [30], the number of steps is estimated to be between two and four. Further, it appears that the concentration of EB along the GTP-cap region of the MT decreases with increasing age of a MT, where age is measured at the time from a rescue event. These results indicate that the GTP-cap, which is recognized by EB proteins [1, 5, 27, 35], also decreases with age. One additional feature of the Hinow model [17] is that it describes the time evolution of MT GTP-cap lengths in growing MTs, as well as the length distributions for growing and shortening MTs. It is for this reason that we choose the modeling framework of Hinow *et al.* [17] as a basis for our study. Specifically, to incorporate MT aging into a description for MT dynamic instability, we require information about MT GTP-cap size.

According to the results of Mohan *et al.* [30], MT aging is a process that most likely exists due to fluctuations in the GTP hydrolysis rate, rather than a change in GTP-tubulin addition (*i.e.*, the MT growth rate) (see also Fig. 2). Such results were also confirmed in cells, since the addition of MT targeting drugs cause decreases in the concentration of EB1 along the growing ends of MTs, and work to induce MT catastrophes at concentrations that do not affect the MT growth rate [34]. Although hydrolysis is one of the primary mechanisms involved in MT catastrophe, its' mechanism has not yet been fully elucidated. Thus, a better description of hydrolysis is needed to accurately describe MT dynamic instability. Many computational and analytical models of MT dynamic instability have been developed to describe how the hydrolysis process might work. Some examples include: random hydrolysis, vectorial hydrolysis, or a combination of both random and vectorial hydrolysis [4, 16, 17, 32, 33]. To complement our continuous modeling approach, we choose a vectorial description of GTP-tubulin hydrolysis. However, we have extended on previous models by incorporating MT age-dependence, as well as a delay that accounts for the incorporation of GTP-tubulin into a growing MT. More precisely, we assume that the hydrolysis rate is an increasing piece-wise function of MT age. In particular, like [30] and as illustrated in Figure 2, we assume that hydrolysis increases in two to four steps, where at each step the hydrolysis is constant and higher in value than the previous step. Further, we assume that between each step, the hydrolysis increases linearly over a short period of time Δa. In this modeling framework, the MT age is defined as either the time after a MT rescue, or the time from nucleation (for MTs that do not undergo a catastrophe). We emphasize that our new modeling approach enables us to more precisely define MT catastrophe frequency as described in biological experiments [18].

Our complete model, based on the approach of Hinow and al. [17], incorporates a system of transport equations to describe time- and length- changes in populations of growing and shortening MTs (as well as changes in the GTP-cap lengths for growing MTs), and a system of ordinary differential equations (ODEs) to describe the time evolution of concentrations of free GTP and GDP-tubulin. We justify the use of an ODE system to describe the evolution of free tubulin by assuming that free tubulin diffusion is much faster than the rate at

which tubulin is incorporated back into a growing MT (thus, tubulin is distributed homogeneously throughout the domain).

Extending on the approach described in [17], not only do we keep track of both MT and GTP-cap lengths, but we also keep track of the MT "age". The new variable "age" will allow us to take into account the dependence of MT age on the GTP-tubulin hydrolysis process. Further, we incorporate a more realistic description for the MT growth rate, one that includes the critical tubulin concentration threshold under which MTs do not grow, and above which the MT growth rate saturates.

Our results show that the incorporation of MT age into our model does affect MT dynamics. Consistent with experiment, results from simulations illustrate how the aging process leads to an increase in the rate of GTP-tubulin hydrolysis for older MTs, as well as increases in catastrophe frequency.

Outline. First, in Section 2 of this paper, we describe the development of our modeling approach. Next, in Section 3, we give details as to how we select our model parameters. In Section 4, we illustrate and analyze the numerical results of our model and in Section 5 we discuss these results. Finally, in the appendix, we provide a detailed description of the finite volume method presented in this paper. Here, we prove the our numerical scheme ensures the preservation of tubulin at the discrete level.

2. CONTINUOUS MODEL OF MT DYNAMICS

We propose a mathematical model of MT dynamic instability based on the continuous approach of Hinow *et al.* [17]. The novelty of our approach is that each MT is characterized by the elapsed time since the last instance of rescue or nucleation, a property we call "age". The addition of age allows us to simulate the impact of MT aging on MT dynamics. MT dynamics are generated by evolutions of the quantities of free GTP-tubulin (described by $t \to p(t)$) and free GDP-tubulin (described by $t \to q(t)$), and by the evolution of the MT population. We distinguish between growing and shrinking MT populations, where MTs in a state of depolymerization are described by the density $v(t, \cdot)$ and those that are in a state of growth are described by $u(t, \cdot, \cdot, \cdot)$. MTs in a state of depolymerization do not possess a GTP stabilizing cap, and so this population is described by one space variable x, corresponding to the length of a MT. A growing MT is characterized by its length x, its cap-size z, and its age a. Age has the dimension of time and starts from zero at the time a MT undergoes a rescue or nucleation. The state space for this population is defined by $Z = \{(a, x, z) \in \mathbb{R}^3 : a > 0, \ x > z > 0\}$.

2.1. Model for growing MTs

The time evolution of MTs in a state of growing is described by the transport equation

$$u_t + u_a + div_{xz}(B(t, a)u) = 0, \quad B(t, a) = \begin{pmatrix} \gamma_{\text{pol}}(p(t)) \\ \gamma_{\text{pol}}(p(t)) - \gamma_{\text{hydro}}(a) \end{pmatrix}, \quad (2.1)$$

where the subscript xz of the divergence operator designates that it acts as a 2D operator, $\gamma_{\text{pol}}(p)$ is the MT growth rate (or rate of polymerization), and $\gamma_{\text{hydro}}(a)$ is the rate of progression of the front the divides the GDP and GTP-tubulin regions. We will refer to this rate as the hydrolysis rate. We denote the balance between these two rates as $R(t, a) = (\gamma_{\text{pol}}(p(t)) - \gamma_{\text{hydro}}(a))$, where this balance corresponds to the growth rate of a GTP-cap at time t for a MT of age a.

We now consider the shape of the MT growth rate and hydrolysis curves. Figure 1(left) describes the MT growth rate, which is known to be proportional to the GTP-tubulin concentration, saturating at high values of tubulin concentration. We denote the saturating value as p_s. Below a critical tubulin concentration, which we denote by p_c, this rate is zero. Thus, γ_{pol} can be represented by a piece-wise linear profile

$$\gamma_{\text{pol}}(p) = \alpha_{\text{pol}} * (p > p_s) + \left(\alpha_{\text{pol}} \frac{p - p_c}{p_s - p_c}\right) * (p_c < p < p_s), \quad (2.2)$$

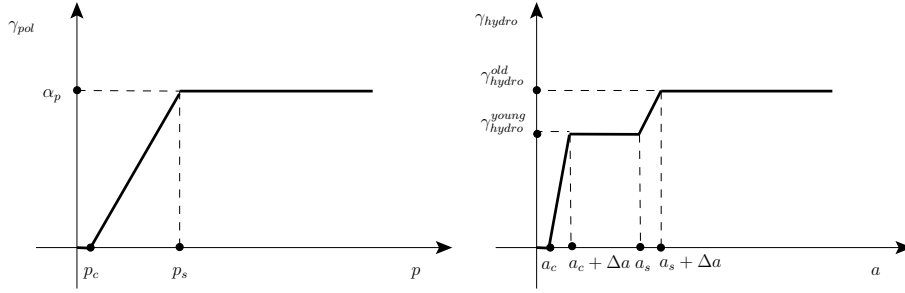where the parameter α_{pol} is the maximum MT growth rate.

FIGURE 1. *Left*: illustration of the function describing the MT growth rate γ_{pol}. *Right*: illustration of the function describing the rate of hydrolysis γ_{hydro}.

In our model, aging of a MT is caused by the acceleration of hydrolysis during MT growth. Accordingly, the function γ_{hydro}, illustrated in Figure 1(*right*), is chosen to be an increasing linear piece-wise function with two layers $\gamma_{\text{hydro}}^{\text{young}}$ and $\gamma_{\text{hydro}}^{\text{old}}$. The value $\gamma_{\text{hydro}}^{\text{young}}$ is the smaller hydrolysis rate (for young MTs) and the value $\gamma_{\text{hydro}}^{\text{old}}$ is the higher hydrolysis rate (for old MTs).

$$\gamma_{\text{hydro}}(a) = \left(\gamma_{\text{hydro}}^{\text{young}} \frac{a - a_c}{\Delta a} \right) * (a_c < a < a_c + \Delta a) + \gamma_{\text{hydro}}^{\text{young}} * (a_c + \Delta a < a < a_s)$$

$$+ \left((\gamma_{\text{hydro}}^{\text{old}} - \gamma_{\text{hydro}}^{\text{young}}) \frac{(a - a_s)}{\Delta a} + \gamma_{\text{hydro}}^{\text{young}} \right) * (a_s < a < a_s + \Delta a) + \gamma_{\text{hydro}}^{\text{old}} * (a_s + \Delta a < a). \quad (2.3)$$

The parameter a_c is the necessary time for the first freshly incorporated GTP-tubulin, after a rescue event, to be hydrolyzed to GDP-tubulin [23, 27, 31, 34]. It is at this time that the aging effect is initiated. Here, the parameter Δa is very small, and corresponds to the transition time between each stage of the aging effect. The parameter a_s is defined as the age at which MTs undergo aging effects, resulting in an increase of the hydrolysis rate up to the maximum value $\gamma_{\text{hydro}}^{\text{old}}$. It is clear from our age-dependent definition of hydrolysis, $\gamma_{\text{hydro}}(a)$, that older MTs with large GTP-caps lose their caps faster than younger MTs.

The domain in consideration, Z, for the concentration $u(t, \cdot, \cdot, \cdot)$, has a prismatic form that is limited by the surfaces $\Gamma_1 = \{a > 0, x > 0, z = x\}$, $\Gamma_2 = \{a > 0, x > 0, z = 0\}$ and $\Gamma_3 = \{a = 0, x > 0, z > 0\}$. We assume that the equation (2.1) is endowed with a boundary condition when the inflow flux $\tilde{B} = (B(t, a), 1)^T \cdot n_i$ is positive, where n_i is the internal normal vector to the surface Γ_i. On Γ_1, we have $\tilde{B} \cdot n_1 = \gamma_{\text{hydro}}(a) \geq 0$. Hence, there is an inflow through the surface Γ_1 that corresponds to freshly nucleated MTs that are composed of GTP-tubulin dimers. On Γ_1, the boundary condition takes the form

$$\gamma_{\text{hydro}}(a) u(t, a, x, x) = \mathcal{N}(p(t)) \psi(x) \Theta(a), \ x \in [0, \infty), \ a \in [0, \infty), \ t \in [0, \infty), \quad (2.4)$$

where we define $\mathcal{N}(p) = \mu p^\nu$. Here, μ is a nucleation rate and ν is the number of GTP-tubulin dimers sufficient for the nucleation of a single MT (here, we take $\nu = 2$).

We define two Dirac-type non-negative functions Θ and ψ such that

$$\int_0^\infty \Theta(a) da = 1 \text{ and } \int_0^\infty x \psi(x) = 1, \quad (2.5)$$

with Θ and ψ supported on supp $\Theta = (0, a_0)$ and supp $\psi = (0, x_0)$, respectively. The function $\psi(x)$ defines the normalized MT length distribution.

Through the boundary Γ_2, MTs can either leave the domain if they undergo a catastrophe, or return to a state of polymerization by undergoing a rescue. If there exists a pair (t, a) such that $R(t, a) < 0$, we say that MTs are in a phase where catastrophes can occur. Similarly, if there exists a pair (t, a) such that $R(t, a) > 0$,

MTs are in the phase where rescues can occur. In contrast to the model of Hinow *et al.* [17], we can have MTs in two of these phases simultaneously, due to the addition of the aging effect. In the case of a catastrophe, the flux $\tilde{B}(t,a) \cdot n_2 = R(t,a)$ is negative, therefore we do not need boundary conditions for MTs that switch to a state of depolymerization. In the case of a rescue event, the flux $\tilde{B}(t,a) \cdot n_2$ is positive when $R(t,a) > 0$. We suggest that rescue events occur in a subset of the plane Γ_2, defined as the narrow stripe $(0,a_0)$, as we assumed in the previous case for the boundary condition on the surface Γ_1. Also, this makes sense, as there is no flux into the domain Z through the plane $a = 0$. To write the corresponding boundary condition, we make use of the Dirac-type function $\Theta(a)$ and assume that MTs return to a state of polymerization with an age between $(0,a_0)$.

$$R(t,a)u(t,a,x,0) = \Theta(a)\lambda v(t,x), \text{ if } R(t,a) > 0, \ t \in [0,\infty), \ a \in [0,\infty), \ x \in [0,\infty) \tag{2.6}$$

Here, λ characterizes the propensity for shrinking MTs to be rescued.

We remark that as $\tilde{B} \cdot n_3 = 1$ is positive on the face Γ_3, then we do need to provide a condition on the inflow through Γ_3. Here, we impose u equal to zero such that

$$u(t,0,x,z) = 0, \quad t \in [0,\infty), \ x \in [0,\infty), \ z \in (0,\infty). \tag{2.7}$$

2.2. Models for shortening MTs, and the concentrations of free GTP- and GDP-tubulin

The equation for the density of shrinking MTs is given by

$$v_t - \gamma_{\text{depol}}v_x = -\int_0^\infty R(t,a)u(t,a,x,0)\mathrm{d}a = -I_{v\to u}(t,x) + I_{u\to v}(t,x), \tag{2.8}$$

where the parameter γ_{depol} is the rate of depolymerization of MTs,

$$I_{v\to u}(t,x) = \int_0^\infty R(t,a)^+ u(t,a,x,0)\mathrm{d}a \quad \text{and} \quad I_{u\to v}(t,x) = \int_0^\infty R(t,a)^- u(t,a,x,0)\mathrm{d}a.$$

Superscripts $+$ and $-$ are used to denote the operators

$$x^+ = \frac{1}{2}\left(x + |x|\right) \text{and} \quad x^- = \frac{1}{2}\left(-x + |x|\right). \tag{2.9}$$

The two terms on the right-hand side of (2.8) correspond to the influx of MTs undergoing catastrophes and/or the outflux of MTs undergoing rescue events.

In [20], it was shown that fluctuations in GTP-tubulin concentration is an important consideration when modeling MT dynamics. It is known that this quantity decreases due its consumption during MT growth and the MT nucleation process. Also, this quantity increases due to the recycling reaction of GDP-tubulin into GTP-tubulin. Thus, we say that the function $p(t)$ satisfies the equation

$$p_t = -\gamma_{\text{pol}}(p)I_{p\to u}(t) + \kappa q - \mathcal{N}(p), \tag{2.10}$$

where

$$I_{p\to u}(t) = \int\limits_0^\infty \int\limits_0^\infty \int\limits_0^x u(t,a,x,z)\mathrm{d}z \, \mathrm{d}x \, \mathrm{d}a \tag{2.11}$$

is the number of growing MTs, κ is the recycling rate of GDP- into GTP-tubulin (which we will continue to refer to as the GDP/GTP recycling rate), and $\mathcal{N}(p)$ describes the uptake of GTP-tubulin due to nucleation.

The equation for free GDP-tubulin $q(t)$ takes the form

$$q_t = \gamma_{\text{depol}}I_{v\to q}(t) - \kappa q, \tag{2.12}$$

where the first term corresponds to an inflow of GDP-tubulin from shortening MTs (which are assumed to only consist of GDP tubulin), and

$$I_{v \to q}(t) = \int\limits_{0}^{\infty} v(t,x) \mathrm{d}x \tag{2.13}$$

corresponds to the number of shortening MTs. The second term corresponds to GDP/GTP recycling. Here, we assume that there is a constant supply of chemical energy, so that the GDP/GTP recycling rate κ remains fixed for the entirety of each simulation.

2.3. Conservation of tubulin

From the model described by equations (2.1), (2.8), (2.10), and (2.12), one can show that the total amount of tubulin in the system is conserved. A similar result was proven by Hinow *et al.* [17]. Lemma 2.1 describes this property.

Lemma 2.1 (Conservation of tubulin). *The total mass of tubulin in the system, that is a sum of free GTP- and GDP-tubulin, and the mass of tubulin contained in MTs is given by*

$$\chi(t) = p(t) + q(t) + L_v(t) + L_u(t),$$

and is constant. That is, $\chi'(t) = 0$. Here, $L_v(t) = \int\limits_{0}^{\infty} x v(t,x) \mathrm{d}x$ is the total tubulin in shortening MTs and $L_u(t) = \int\limits_{0}^{\infty} \int\limits_{0}^{\infty} \int\limits_{0}^{x} x u(t,a,x,z) \mathrm{d}z \, ; \mathrm{d}x \, \mathrm{d}a$ is the total tubulin in growing MTs.

2.4. Mathematical expressions for experimental observations

Here, we describe mathematical expressions for quantities that can be observed experimentally. Such expressions are important as they allow us to compare the results of our simulations with experimental results. The quantities we consider here are: the number of MTs in growing and shortening states, the catastrophe frequency (temporal and spatial-based), the average length of MTs in growing and shortening states, the average hydrolysis rate, and the decoration time.

- The number of MTs in states of polymerization and depolymerization at time t are

$$I_{p \to v}(t) \quad \text{and} \quad I_{q \to v}(t).$$

These expressions are defined in equations (2.11) and (2.13).

- The average temporal-based catastrophe frequency (in $\min^{-1}$) is

$$F_{\text{cat}}^{\text{temp}}(t) = \frac{\int\limits_{0}^{\infty} \int\limits_{0}^{t} \frac{1}{a} \mathbf{1}_{R(t,a)<0} u(t,a,x,0) \mathrm{d}a \, \mathrm{d}x}{\int\limits_{0}^{\infty} \int\limits_{0}^{t} \mathbf{1}_{R(t,a)<0} u(t,a,x,0) \mathrm{d}a \, \mathrm{d}x}.$$

where $\mathbf{1}_A$ stands for the characteristic function of the set A. In experiment, the average time-based catastrophe frequency can be defined as the total number of catastrophe events divided by the total time MTs spend growing (averaged over a population of MTs).

- The average spatial-based catastrophe frequency (in $\mu\mathrm{m}^{-1}$) is

$$F_{\mathrm{cat}}^{\mathrm{spa}}(t) = \frac{\int\limits_0^\infty \int\limits_0^t \frac{1}{\int_0^a \gamma_{\mathrm{pol}}(t-a+s)\,\mathrm{d}s} \mathbf{1}_{R(t,a)<0} u(t,a,x,0)\mathrm{d}a\,\mathrm{d}x}{\int\limits_0^\infty \int\limits_0^t \mathbf{1}_{R(t,a)<0} u(t,a,x,0)\mathrm{d}a\,\mathrm{d}x}.$$

Note that $\int_0^a \gamma_{\mathrm{pol}}(t-a+s)ds$ is the increase in length of a MT at time t from time $t-a$ (time from rescue). Experimentally, the length-based catastrophe frequency is defined as the total number of catastrophe events divided by the length to which MTs grow before undergoing a catastrophe.

- The average length of MTs in states of polymerization and depolymerization, and the average length of the MT GTP-cap (in $\mu\mathrm{m}$) are given by

$$L_u^{\mathrm{av}}(t) = \frac{L_u(t)}{I_{p\to u}(t)}, \quad L_v^{\mathrm{av}}(t) = \frac{L_v(t)}{I_{q\to v}(t)}, \quad \text{and} \quad L_{\mathrm{cap}}^{\mathrm{av}}(t) = \frac{\iiint\limits_Z z u(t,a,x,z)\mathrm{d}a\,\mathrm{d}z\,\mathrm{d}x}{I_{p\to u}(t)},$$

where $L_u(t)$ and $L_v(t)$ are described in Lemma 2.1.

- The average rate of hydrolysis for the population of MTs in a state of polymerization (in $\mu\mathrm{m}\ \mathrm{min}^{-1}$) is

$$\gamma_{\mathrm{hydro}}^{\mathrm{av}}(t) = \frac{\iiint\limits_Z \gamma_{\mathrm{hydro}}(a)u(t,a,x,z)\mathrm{d}a\,\mathrm{d}z\,\mathrm{d}x}{I_{p\to u}(t)}.$$

- The decoration time (in seconds) is

$$T_{\mathrm{deco}}(t) = \frac{L_{\mathrm{cap}}^{\mathrm{av}}(t)}{\gamma_{\mathrm{pol}}(p(t))}.$$

In particular, the decoration time is the mean time required for GTP-tubulin to be hydrolyzed to GDP-tubulin after incorporation into a MT [13]. In biological experiments [23, 34] and in our simulations, such a quantity is evaluated at steady-state.

3. NUMERICAL DETAILS

In this section, we outline the numerical details of our modeling approach. A detailled description of the scheme is given in appendix. In Section 3.1, we describe how to determine units for all model parameters. Finally, in Section 3.2, we describe how to determine appropriate ranges for all model parameters.

3.1. Parameter units

In our model, quantities for GTP- and GDP-tubulin (p and q) have units of measure in $\mu\mathrm{M}$ (micromole per liter), while MT length x and GTP-cap size z are measured in $\mu\mathrm{m}$ (micrometer). For simulations, we must convert these quantities to similar units of measure. In particular, we convert $\mu\mathrm{M}$ to $\mu\mathrm{m} \cdot \mathrm{L}^{-1}$. In $1\,\mu\mathrm{mol}$ of tubulin there are $10^{-6} \times N_A = 6.022 \times 10^{17}$ molecules of tubulin, where N_A is the Avagadro constant.

Here, we approximate a MT as a single protofilament. To use the parameters of kinetics measured for a MT with 13 protofilaments, we assume that a unit of length in the model is given by

$$l_{\mathrm{unit}} = 8.12 \times 10^{-3}/13 = 6.2462 \times 10^{-4}[\mu\mathrm{m}],$$

where $8.12\ n\mathrm{m}$ is the approximate length of one dimer. Thus, the factor of conversion from $\mu\mathrm{mol}$ to $\mu\mathrm{m}$ is

$$conv = (6.022 \times 10^{17} \times l_{\mathrm{unit}}) = 3.76 \times 10^{14}\ \mu\mathrm{m} \cdot \mathrm{L}^{-1}, \tag{3.1}$$

TABLE 1. List of parameters and their values used as model input.

Parameter	Values	Meaning	Source
p_c	0–3 μM	Critical tubulin concentration	[28]
p_s	12–18 μM	Saturation tubulin concentration	[This paper]
α_{pol}	25–40 $\frac{\mu\text{m}}{\mu\text{M}\cdot\text{min}}$	Growth rate parameter	[34],[This paper]
a_c	1.2–9 s	The age at which MTs undergo the first hydrolysis after tubulin incorporation	[23]
a_s	12–60 s	The age at which MTs undergo a maximum hydrolysis effect	[34]
Δa	6×10^{-3} s	Time between the minimum and maximum aging effect	[This paper]
$\gamma_{\text{hydro}}^{\text{young}}$	3-7 $\frac{\mu\text{m}}{\text{min}}$	Hydrolysis rate of young MT (normal hydrolysis rate)	[This paper]
$\gamma_{\text{hydro}}^{\text{old}}$	4–10 $\frac{\mu\text{m}}{\text{min}}$	Hydrolysis rate of old MTs (i.e. aging effect)	[This paper]
γ_{depol}	3–36 $\frac{\mu\text{m}}{\text{min}}$	Rate of depolymerization	[34]
λ	3–10 $\frac{1}{\text{min}}$	Rescue rate	[18]
μ	5.9×10^{-3} $\frac{1}{\mu\text{M}\cdot\text{min}}$	Nucleation parameter	[17]
κ	0.5–10 $\frac{1}{\text{min}}$	GDP/GTP recycling rate	[17]

and estimates the number of MTs contained within a cell of MT concentration equal to 1μM. We assume that the range of a MT length is between 20 and 100 μm [15]. By using the factor of conversion (3.1), this range can be expressed as a concentration between $3.76 \times 10^{12} - 1.88 \times 10^{13}$ MTs per liter.

To make an assessment of the concentration of MTs, consider a cell of cylindrical form with radius 10 μm and height 2 μm. The volume of such a cell is

$$\pi \times 10^2 \times 2\mu\text{m}^3 = 600 \,\mu\text{m}^3 = 6 \times 10^{-16}\text{m}^3 = 6 \times 10^{-13} \text{ L}.$$

Thus, within this volume a concentration of tubulin equal to 1 μM corresponds to approximately $2 - 10$ MTs.

3.2. Choice of parameter ranges

The dynamics of the system is driven by the set of parameters

$$p_c, \, p_s, \, \alpha_{\text{pol}}, \, a_c, \, a_s, \, \Delta a, \, \gamma_{\text{hydro}}^{\text{young}}, \, \gamma_{\text{hydro}}^{\text{old}}, \, \gamma_{\text{depol}}, \, \lambda, \, \mu, \, \kappa.$$

These parameters, as well as their range of values and meaning are listed in Table 1.

From biological observations of MTs dynamics, it is possible to define ranges for some of the model parameters described in Table 1. In particular, values for the parameters p_c, γ_{depol}, a_s, and a_c can be found in the literature. The other parameters can be estimated by obtaining appropriate values for quantities that can be directly compared with experiment. These quantities include the MT growth rate, catastrophe frequencies, and the length of the EB1-GTP cap at equilibrium [18]. From here on, we refer to these quantities as the *simulated observables.*

The rate of depolymerization γ_{depol} is directly linked to the shortening rate, where its range (in the absence of drugs) is between $3 - 36$ μm min^{-1} [34].

The range for p_c is described in [28] and is found to be between 0–3 μm L^{-1}. The other parameters that define γ_{pol} (see Eq. (2.2)), are not found experimentally. However, we do have information for the MT growth rate at equilibrium $\gamma_{\text{pol}}(p^\infty)$. In particular, in one study (which we will use to calibrate our model), this rate is found to be between 3–7 μm min^{-1} [34]. To obtain desired MT growth rates (as we will show later in the Results Section), we choose α_{pol} to be between 25–40 μm min^{-1} μM^{-1} and p_s to be between $12 - 18$ μm L^{-1}.

For the parameters defining the rate of hydrolysis γ_{hydro} (recall Eq. (2.3)) we choose a_c to be between $0.02 - 0.15$ min [23]. The parameter a_s can be estimated using data taken from kymographs (see Fig. 2, Ref. [34]), and ranges between $12 - 60$ seconds. A kymograph is used to show the growth trajectory of a single MT *in vitro*, and is read from top to bottom. We see that each MT (shown in the left and center panel of Fig. 2)
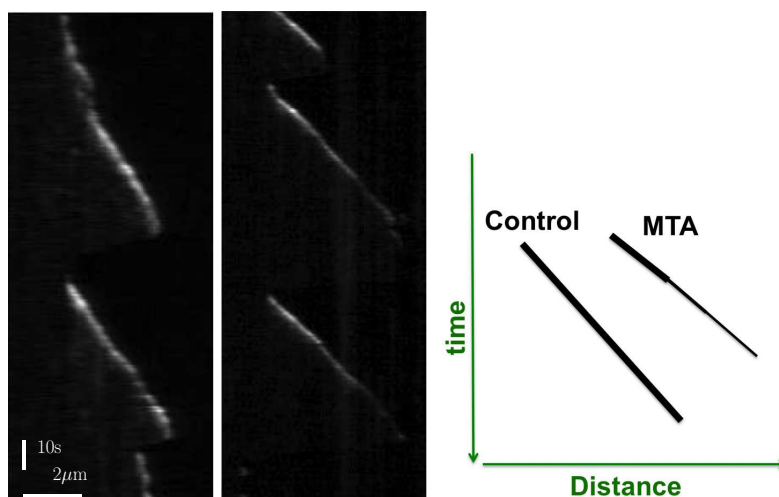
FIGURE 2. Kymographs that highlight growth and shortening of a single MT. MT tips are highlighted by green fluorescent protein (GFP) tagged EB3 [34]. *Left*: a kymograph of a GFP EB3-tip tracking assay in the absence of drugs. Experimental conditions are: GFP EB3: 75 μM, cowtubulin: 15 μM, KCl: 50 μM, temp: 37°C. *Center*: a kymograph in the presence of a low concentration of paclitaxel 100 μM. A time-dependent decrease of the EB-stabilizing cap is observed. *Right*: a graphical illustration of the kymographs shown in (*left*) and (*center*).

grows at a relatively constant rate, while undergoing a number of shortening events. The left panel of Figure 2 illustrates a MT in a control setting [34], while the center panel illustrates a MT growing in the presence of paclitaxel, a MT stabilizing drug. Here, you can see that the MT grows to a longer length over a shorter period of time in the presence of paclitaxel. The right panel is a cartoon illustration used to highlight the change in the slope of the MT growth curve when paclitaxel is added.

Numerical simulations show that the mean rate of hydrolysis is very close to the equilibrium growth rate. Thus, we calibrate $\gamma_{\text{hydro}}^{\text{young}}$ and $\gamma_{\text{hydro}}^{\text{old}}$ according to the growth rates given in the literature [34]. That is, we choose the ranges $3-7$ μm min^{-1} and $4-10$ μm min^{-1} for $\gamma_{\text{hydro}}^{\text{young}}$ and $\gamma_{\text{hydro}}^{\text{old}}$, respectively.

The parameter λ (propensity of rescue) is not directly linked to the rescue frequency as estimated in biological experiments [18]. We adjust this parameter to be $5-10$ min^{-1} by obtaining a value for the catastrophe frequency at equilibrium that is similar to experiment [34].

The value of $\mu = 5.9 \times 10^{-3} \mu\text{M}^{-1}$ min^{-1} is taken from [17]. Also, we examine a wide range of values for the GDP/GTP recycling parameter κ, choosing values between $0.5-10$ min^{-1}.

4. RESULTS

First, in Section 4.1, we describe results of MT dynamics using parameters similar to those found in experimental settings. We show that our simulation results are consistent with experiment and refer to this test as our control. Then, in Section 4.2, we vary model parameters to show which parameters play a significant role in altering MT dynamics.

4.1. A control test: *in silico* observations

The values for model parameters used in our reference test (simulated control test) are listed in Table 2. As a comparison to experiment, we list simulated values for the MT growth rate and the spatial and temporal catastrophe frequencies in Table 3, alongside their corresponding experimental values determined by Pagano

TABLE 2. Parameters for the "control" test.

Parameter	p_c	p_s	α_{pol}	a_c	a_s	δa	$\gamma_{\text{hydro}}^{\text{young}}$	$\gamma_{\text{hydro}}^{\text{old}}$
SI units	μM	μM	μm min$^{-1}\mu$M^{-1}	s	s	s	μm min^{-1}	μm min^{-1}
Value	2	15	32	6	60	6×10^{-3}	3.7	4.3

	Parameter	γ_{depol}	λ	μ	κ		
	SI units	μm min^{-1}	min^{-1}	μM^{-1}min^{-1}	min^{-1}		
	Value	19	5	5.9e-3	2.4		

TABLE 3. Comparison of model output with experimental data.

	$\gamma_{\text{pol}}(p^\infty)$	γ_{depol}	$F_{\text{cat}}^{\text{temp}}$	$F_{\text{cat}}^{\text{spa}}$
SI units	[μm min$^{-1}\mu$M^{-1}]	[μm min^{-1}]	[min^{-1}]	[μm^{-1}]
Experimental control [34]	3.87	19.09	1.72	0.42
Simulated "control" test	3.23	19(fixed)	1.88	0.58

et al. [34]. From this table, we see that the output of the control test is consistent with biological observations. As stated previously, the parameters a_s, γ_{depoly}, as well as the initial condition of the simulation are the taken from the experiment of Pagano *et al.* [34]. All other model parameter inputs were not directly taken from the experiment of Pagano *et al.* [34], since they were not recorded. However, we selected each parameter from a range of values that have been recorded in similar experiments. Values were selected to calibrate our model, so that our model output matches that of Pagano *et al.* [34].

For all numerical simulations that follow, we choose initial conditions $p(0) = 15$ μM, $q(0) = 0$, $v(0, \cdot) = 0$, and $u(0, \cdot, \cdot, \cdot) = 0$. We choose these conditions since in most *in vitro* experiments, MTs are grown in systems comprised of purely free GTP-tubulin [3, 10, 25]. Also, in all numerical tests carried out, including the control test, nucleation of MTs is switched off (*i.e.*, $\mu = 0$) at $t = 15$ min to avoid the influence of this parameter in our analysis. Switching off nucleation also makes sense from a biological point of view, as it is often the case that nucleation stops in *in vitro* experiments after some time when much of free GTP-tubulin is used up (after the polymer mass increases to a sufficiently high value).

The other simulated observables of MT dynamics at the equilibrium state, such as the average rate of hydrolysis, the average GTP-cap length and the GTP-tubulin decoration time, as well as the simulated observables summarized in Table 3 (the MT growth rate and the catastrophe frequencies), are summarized in the first rows of Tables 4 and 5.

Figure 3 corresponds to the simulation output for our control test. The curves from Figures 3a, 3c, 3d and 3f show that the system reaches an equilibrium state after a short period of time. Figure 3b illustrates that the average lengths of both growing and shortening MT populations are less than 50 μm, and the average GTP cap becomes very small, reaching an equilibrium during the second part of simulation ($t > 15$ min). This agrees with experimental data [15, 35]. In Figure 3f, we illustrate the decoration time. We split the graph into two pieces to more easily visualize the results (*i.e.*, the values in the first part of the simulation are much larger than those in the second part of the simulation). The value at equilibrium (approximately 10 s), is close to what has been observed experimentally [34].

In Figure 3e, we plot three curves that correspond to the rate of MT polymerization, the average rate of GTP hydrolysis, and the ratio of the temporal to spatial catastrophe frequencies (which we denote as Temp-to-Spa frequency ratio). The two curves that correspond to the growth rate and the Temp-to-Spa frequency ratio coincide for much of the simulation, as we expected, confirming our choice of formulae for both frequencies.

Also, from Figure 3e, we observe a relationship between the rate of polymerization and the rate of hydrolysis. That is, the relative difference $(\gamma_{\text{pol}} - \gamma_{\text{hydro}}^{\text{av}})/\gamma_{\text{pol}}$ between the mean growth rate and the mean rate of hydrolysis

TABLE 4. Changes in simulated observables: growth rate and GTP hydrolysis rate at steady-state.

	$\gamma_{\mathrm{pol}}(p^\infty)$		$\gamma_{\mathrm{hydro}}^{\mathrm{av}}$		$\frac{\gamma_{\mathrm{hydro}}^{\mathrm{av}}-\gamma_{\mathrm{pol}}}{\gamma_{\mathrm{pol}}}$
simulated ctrl	3.23		3.65		13%
param changed from ctrl	value	change	value	change	value
$a_c = 1.2 \downarrow$	3.43 ↑	6.2%	3.89 ↑	6.6%	13.4%
$a_c = 9 \uparrow$	3.13 ↓	-3.1%	3.54 ↓	-3.0%	13.1%
$a_s = 12\downarrow$	3.47 ↑	7.1%	3.94 ↑	7.9%	13.5%
$\gamma_{\mathrm{hydro}}^{\mathrm{old}} = 7.3 \uparrow$	3.53 ↑	9.3%	4.00 ↑	9.6%	13.3%
$\gamma_{\mathrm{hydro}}^{\mathrm{young}} = 6.7 \uparrow$ $\gamma_{\mathrm{hydro}}^{\mathrm{old}} = 7.3 \uparrow$	5.34 ↑	65.3%	6.04 ↑	65.5%	13.1%
$a_s = 12 \downarrow$ $\gamma_{\mathrm{hydro}}^{\mathrm{old}} = 7.3 \uparrow$	5.30 ↑	64.0%	6.0 ↑	64.3%	13.2%
$\gamma_{\mathrm{depol}} = 9 \downarrow$	2.81 ↓	–13%	3.59 ↓	-1.6%	27.8%
$\gamma_{\mathrm{depol}} = 29 \uparrow$	3.48 ↑	7.7%	3.79 ↑	3.8 %	8.9%
$\lambda = 10 \uparrow$	2.67 ↓	–17.3%	3.37 ↓	-7.7%	26.2%
$\lambda = 3 \downarrow$	3.57 ↑	10.5%	3.86 ↑	5.7%	8.1%
$\alpha_{\mathrm{pol}} = 25 \downarrow$	3.23	0%	3.65	0%	13.0%
$\alpha_{\mathrm{pol}} = 40 \uparrow$	3.23	0%	3.65	0%	13.0%
$p_s = 4 \downarrow$	3.23	0%	3.65	0%	13.0%
$p_s = 4 \downarrow$ $\alpha_{\mathrm{pol}} = 5 \downarrow$	3.23	0%	3.65	0%	13.0%
$\kappa = 10 \uparrow$	3.22	0%	3.65	0%	13.3%
$\kappa = 0.5 \downarrow$	3.23	0%	3.66	0%	13.3%

appears to be small and almost constant (see values in Tab. 4), suggesting some kind of regulation of one parameter by the other.

4.2. Influence of the parameter variation on MT dynamics

After completing the model calibration, we study the influence of each parameter on MT dynamics. As stated previously, the first row in Tables 4 and 5 correspond to the simulated observables obtained from our control test. Each of the following rows of Tables 4 and 5 correspond to a numerical test where we change one or multiple values of the parameters from its control value at $t = 15$ min. The list of parameter changes (an increase or decrease) are given in the first column, while each row shows the results of the parameter changes (changes from control values are shown as percent changes). Using the information in Tables 4 and 5, we are able to distinguish which parameter (or group of parameters) has a strong effect on MT dynamics.

In Table 4, we show how changes in various model parameters (increases and decreases) affect both the MT growth rate γ_{pol} and the hydrolysis rate $\gamma_{\mathrm{hydro}}^{\mathrm{av}}$ at equilibrium. The changes in the parameters of a_c, a_s and in the rates $\gamma_{\mathrm{hydro}}^{\mathrm{young}}$ and $\gamma_{\mathrm{hydro}}^{\mathrm{old}}$ result in the change in average GTP-hydrolysis rate which is expected. Interestingly, the relative difference between average GTP-hydrolysis rate and the growth speed is affected very little (as shown in the last column of Tab. 4) for these cases. This result suggests that the growth rate is regulated by the resulting average GTP hydrolysis rate. The relative difference between these two values (as shown in the last column of Tab. 4) is affected very little by changes in most of the parameters, except for changes to the rate of MT depolymerization γ_{depol} and the propensity of rescues λ. Here, it is shown that, this difference significantly decreases when the rate of depolymerization decreases or the rescue frequency increases.

The results of Table 5 show that changes to the parameter of critical age a_c have a significant influence on MT dynamics. In particular, a decrease in this parameter to 1.2s (from 6s) increases the time based catastrophe
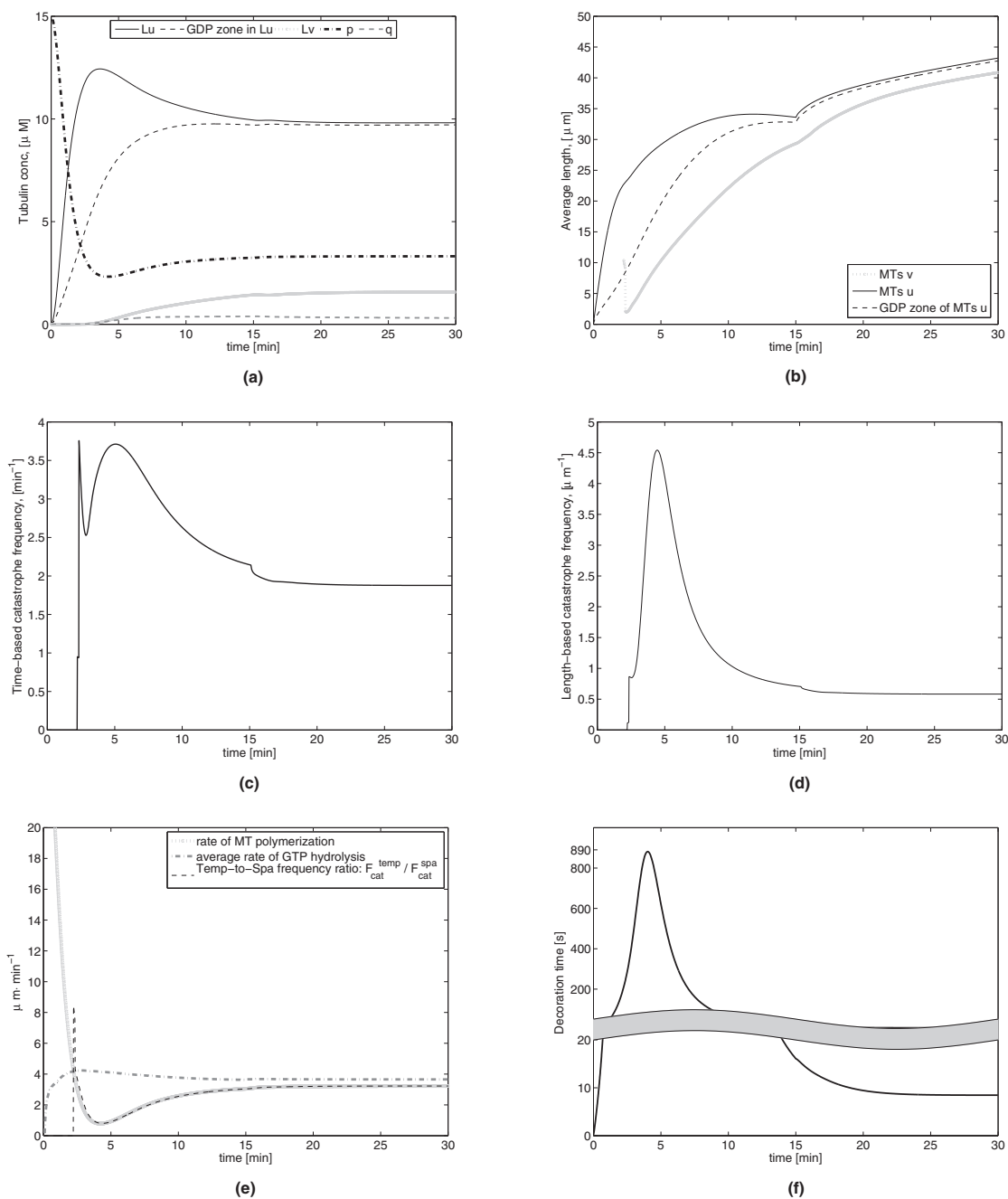
FIGURE 3. Numerical output of the model. (a) Time evolution of the total amount of tubulin in growing MTs, $(t \rightarrow L_u(t))$ and shortening MTs $(t \rightarrow L_v(t))$, total length of GDP zone in growing MT population u, total amount of free GTP-tubulin $(t \rightarrow p(t))$, and of free GDP-tubulin $(t \rightarrow q(t))$; (b) evolution of averaged lengths for both populations of MTs and the average length of the GDP zone; (c) the temporal catastrophe frequency over time; (d) the spatial catastrophe frequency over time; (e) the growth rate of MTs, the Temp-to-Spa frequency ratio, and the average rate of GTP hydrolysis; (f) the MT decoration time (split in two pieces).

TABLE 5. Changes in simulated observables: transition frequencies, length of the GTP-cap and decoration time at steady-state.

	$F_{\text{cat}}^{\text{temp}}$, [min^{-1}]		$F_{\text{cat}}^{\text{spa}}$, [$\mu m^{-1}$]		L_{cap}^{av},[μm]		T_{deco}, [s]	
simulated ctrl	1.88		0.58		0.45		8.46	
param changed								
from ctrl	value	change	value	change	value	change	value	change
$a_c = 1.2 \downarrow$	3.03 ↑	61,2%	0.88 ↑	51.7%	0.25 ↓	−44.4%	4.39↓	—-48.1%
$a_c = 9 \uparrow$	1.61 ↓	−14.4%	0.51 ↓	−12%	0.53 ↑	17.8%	10.20 ↑	20.6%
$a_s = 12 \downarrow$	1.89	0.5%	0.54 ↓	−7%	0.46	2.2%	7.96 ↓	−5.9%
$\gamma_{\text{hydro}}^{\text{old}} = 7.3 \uparrow$	2.20 ↑	17%	0.62 ↑	7%	0.50 ↑	11.1%	8.44 ↓	−0.2%
$\gamma_{\text{hydro}}^{\text{young}} = 6.7 \uparrow$ $\gamma_{\text{hydro}}^{\text{old}} = 7.3 \uparrow$	2.38 ↑	26.6%	0.45 ↓	−22.4%	0.54 ↑	20%	6.09 ↓	−28%
$a_s = 12 \downarrow$ $\gamma_{\text{hydro}}^{\text{old}} = 7.3 \uparrow$	1.84 ↓	−2.1%	0.35 ↓	−39.7%	0.63 ↑	40%	7.18 ↓	−15.1%
$\gamma_{\text{depol}} = 9 \downarrow$	2.96 ↑	57.4%	1.05 ↑	81%	0.33 ↓	−26.7%	6.99 ↓	−17.4%
$\gamma_{\text{depol}} = 29 \uparrow$	1.54 ↓	−18%	0.44 ↓	−24.1%	0.49 ↑	8.9%	8.49 ↑	0.4%
$\lambda = 10 \uparrow$	2.57 ↑	36.7%	0.96 ↑	65.5%	0.42 ↓	−6.7%	9.48 ↑	12%
$\lambda = 3 \downarrow$	1.54 ↓	−18%	0.43 ↓	−25.9%	0.48 ↑	6.7%	7.53 ↓	−11%
$\alpha_{\text{pol}} = 25 \downarrow$	1.88	0%	0.58	0%	0.45	0%	8.46	0%
$\alpha_{\text{pol}} = 40 \uparrow$	1.88	0%	0.58	0%	0.46	2.2%	8.46	0%
$p_s = 4 \downarrow$	1.88	0%	0.58	0%	0.46	2.2%	8.47	0%
$p_s = 4 \downarrow$ $\alpha_{\text{pol}} = 5 \downarrow$	1.88	0%	0.58	0%	0.45	0%	8.46	0%
$\kappa = 10 \uparrow$	1.88	0%	0.58	0%	0.45	0%	8.47	0.1%
$\kappa = 0.5 \downarrow$	1.87	−0.5%	0.58	0%	0.46	2.2%	8.45	−0.1%

frequency ($F_{\text{cat}}^{\text{temp}}$) by 61% and the spatial based catastrophe ($F_{\text{cat}}^{\text{spa}}$) by 52%. Also, we see a decrease in the GTP-tubulin decoration time by 48 %, while the growth rate $\gamma_{\text{pol}}(p^{\infty})$ and the hydrolysis rate $\gamma_{\text{hydro}}^{\text{av}}$ are not significantly affected. We conclude that this parameter is likely to play an important role in regulating MT dynamic instability.

Also, in Table 5, we show that an increase in the parameter $\gamma_{\text{hydro}}^{\text{old}}$ changes only the temporal frequency of catastrophe by a significant amount (17%) (the impact on other parameter values is much smaller). However, if we change this parameter simultaneously with $\gamma_{\text{hydro}}^{\text{young}}$ or a_s, more significant changes are noted. In particular, if we increase the parameter $\gamma_{\text{hydro}}^{\text{old}}$ while increasing $\gamma_{\text{hydro}}^{\text{young}}$ or decreasing a_s, we see that almost all simulated observables change to a large extent. Also, in Table 5, we see significant changes in $\gamma_{\text{pol}}(p^{\infty})$ and $\gamma_{\text{hydro}}^{\text{av}}$, but the value of the relative difference between γ_{pol} and $\gamma_{\text{hydro}}^{\text{av}}$ remains at 13% (similar to the control test).

From Tables 4 and 5, we show that changes in the parameters that define the rate of polymerization (p_s and α_{pol}), as well as changes to the GDP/GTP recycling rate κ, do not change the simulated observables at equilibrium. From Figure 4, we can see that changes to these parameters at $t = 15$ min reorganize the distribution of tubulin in growing MTs, as well as the free tubulin mass, except for the case when $\alpha_{\text{pol}} = 5$ and $p_s = 4$ (see Fig. 4d). We first consider the case where we change the slope of the function γ_{pol} on the segment (p_c, p_s) (see Fig. 1). These changes are illustrated in Figures 4a–4c. In the case of $\alpha_{\text{pol}} = 25$ (see Fig. 4a), the slope of γ_{pol} is decreased, and we can see from Table 6 that the total polymerized tublin mass of both growing and shortening MT populations is decreased at the steady state (recall the steady-state illustrated in Fig. 3a). This results in an increase in the concentration of free GTP-tubulin, induced by depolymerizing MTs. However, this does not result in a change in the value of p^{∞}, or a change in the values of the other simulated observables (from the control test). When we increase the slope of γ_{pol}, by setting $\alpha_{\text{pol}} = 40$ (see Fig. 4b) or by setting $p_s = 4$ (see Fig. 4c), the concentration of free GTP-tubulin decreases at equilibrium (see Tab. 6). However,
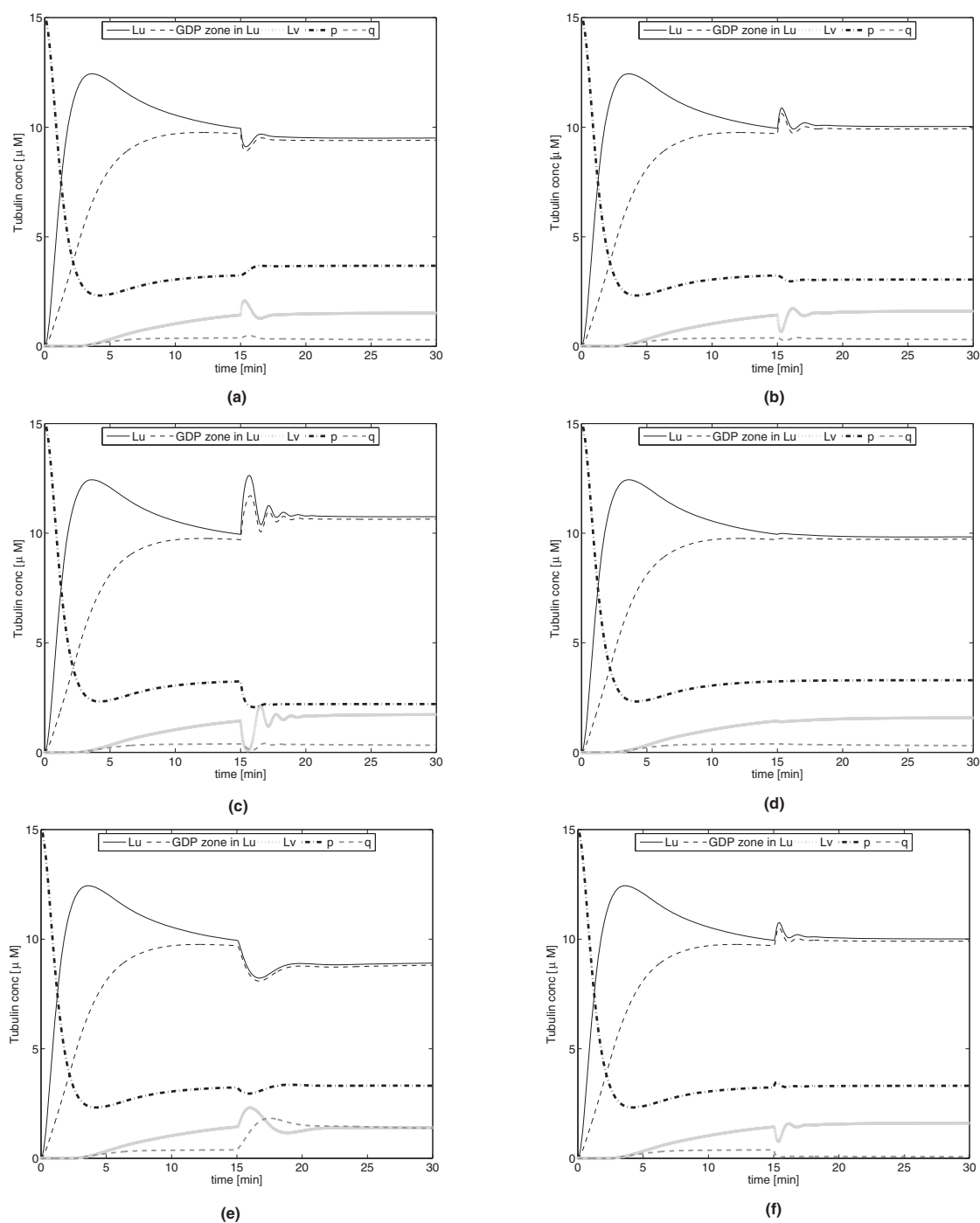
FIGURE 4. Total tubulin mass in MT populations u (L_u) and v (L_v), GDP-tubulin in growing MTs, free GTP-tubulin p, and free GDP-tubulin q for the cases where changing model parameters does not strongly influence simulated observables: (a) $\alpha_{pol} = 25$; (b) $\alpha_{pol} = 40$; (c) $p_s = 4$; (d) $\alpha_{pol} = 5$, $p_s = 4$; (e) $\kappa = 0.5$; (f) $\kappa = 10$.

TABLE 6. Numerical tests and tubulin concentrations at steady-state.

	L_u^∞		L_v^∞		p^∞		$\boldsymbol{q^\infty}$	
simulated ctrl	9.81		1.57		3.31		0.31	
param changed								
from ctrl	value	change	value	change	value	change	value	change
$\alpha_{\mathrm{pol}} = 25 \downarrow$	9.50 $\downarrow$	–3.2%	1.52 $\downarrow$	–3.2%	3.68 $\uparrow$	11.2%	0.30 $\downarrow$	–3.2%
$\alpha_{\mathrm{pol}} = 40 \uparrow$	10.04 $\uparrow$	2.34%	1.61 $\uparrow$	2.5%	3.05 $\downarrow$	-7.9%	0.31	0%
$p_s = 4 \downarrow$	10.75 $\uparrow$	9.6%	1.72 $\uparrow$	9.6%	2.20	–33.5%	0.32 $\downarrow$	3.2%
$p_s = 4 \downarrow$								
$\alpha_{\mathrm{pol}} = 5 \downarrow$	9.83 $\uparrow$	0.2%	1.57	0%	3.29 $\downarrow$	–0.6%	0.31	0%
$\kappa = 0.5 \downarrow$	8.90 $\downarrow$	-9.28%	1.40 $\downarrow$	–10.8%	3.31	0%	1.37 $\uparrow$	341.9%
$\kappa = 10 \uparrow$	10.01 $\uparrow$	2.0%	1.60 $\uparrow$	1.9%	3.31	0%	0.07 $\downarrow$	–77.4%

like in the previous case, the growth rate and the other simulated observables do not change from their control values. In the case where $\alpha_{\mathrm{pol}} = 5$ and $p_s = 4$, the slope of γ_{pol} on the segment (p_c, p_s) remains unchanged. Thus, the system dynamics are the same as those of the control test, as we expected.

For each of the cases described in the previous paragraph, the concentration of free GDP-tubulin does not change much from the control case. In contrast, if we change the value of the recycling parameter κ, changes in the concentration of free GDP-tubulin are more pronounced (see Figs. 4e and 4f). However, there is little change to the other simulated observables. From Table 6, we see that the change of the GDP-tubulin concentration q is due to either an increase or a decrease in the total polymerized tubulin mass, and not as a result of changes in the concentration of free GTP-tubulin p. In particular, the concentration p is maintained at its control value, as is the MT growth rate.

Decreasing of rate of depolymerization γ_{depol} or increasing the propensity of rescue λ leads to a decrease in the growth rate $\gamma_{\mathrm{pol}}(p^\infty)$ by –13% and –17%, respectively. However, in both these cases, the hydrolysis rate $\gamma_{\mathrm{hydro}}^{\mathrm{av}}$ remains nearly fixed (to its control value). This leads to large increases for both time and space-based catastrophe frequency.

5. DISCUSSION AND CONCLUSIONS

In this paper, we developed a novel modeling approach to describe how MT dynamics are affected by the process of MT aging. Extending on the work of Hinow *et al.* [17], we incorporated a new variable to describe the age of growing MTs. By doing so, we were able to define mathematical expressions for the temporal and spatial catastrophe frequency of MTs. Such expressions are important, since these frequencies can be observed experimentally. Thus, we can use these expressions to compare our simulated results with real data. Further, we were able to use known values for these quantities to calibrate other unknown parameters in our model. Data used in our model calibration was based on *in vitro* data from [34], verifying that our model can reproduce biologically realistic results.

The introduction of an aging effect in the hydrolysis rate had significant consequences on MT dynamics. Here, MT age is defined as either the time after a MT rescue, or the time from nucleation, where it is assumed that the hydrolysis rate is an increasing function of MT age. In particular, simulations with decreasing a_s (the age at which MTs undergo aging effects, resulting in an increase in hydrolysis) alone resulted in increases in the growth rate, the rate of hydrolysis, and the time-based catastrophe frequency. Also, increasing $\gamma_{\mathrm{hydro}}^{\mathrm{old}}$ resulted in increases to both catastrophe frequencies, and the hydrolysis rate.

Interestingly, if we varied both a_s and $\gamma_{\mathrm{hydro}}^{\mathrm{old}}$ together (decreasing a_s and increasing $\gamma_{\mathrm{hydro}}^{\mathrm{old}}$), a stronger increase in the MT growth rate and hydrolysis rate was observed. However, unlike the case where we vary each parameter alone, both catastrophe frequencies are decreased.

Moreover, the ratio of the temporal to the spatial catastrophe frequency coincides with the growth rate of MTs, a result that was expected, providing more evidence that our modeling framework provides a good description of MT dynamics. Also, we found that the equilibrium values for the average rate of hydrolysis and the MT growth rate are connected in such a way that changes in the rate of hydrolysis cause changes in the resulting growth rate at equilibrium. This result provides evidence that MT growth and hydrolysis may work to regulate one another.

As stated in the introduction, one of the future objectives of this project is to understand the affect of MTAs on MT dynamics. The study performed here on the influence of the parameters is a first step in understanding this effect. As an example, when we decrease the parameter a_c (the time it takes for newly added GTP-tubulin to be hydrolyzed to GDP-tubulin), there is a significant increase in both the time- and space-based catastrophe frequencies, as well as an increase in the hydrolysis rate. Also, there is a significant decrease in the MT cap length, and the decoration time. These changes are consistent to what is observed when MT destabilizing drugs (such as vinblastine) act on MTs [30]. This results suggests that the action of such a drug may work by acting on the MT aging process.

In future work, we will perform a similar analysis, so as to gain further insight into which model parameters might be directly affected by the addition of other MTAs. Also, as a future consideration, we will explore ways to extend our model to include a mathematical expression for time-based rescue, as this is also a quantity that is calculated in experiments, and is altered by the addition of MTAs.

Appendix A. Finite volume discretization

Here, we propose a finite volume approximation for the system of equations (2.1), (2.8), (2.10), (2.12) that preserves the total tubulin mass at a discrete level. In Section A.2, we describe approximations for the ODEs that describe the time evolution of the concentrations of GTP and GDP-tubulin, and in Sections A.3 and A.4, we describe approximations for the transport equations describing shorting MTs v and growing MTs u, respectively. We made a special attention to the approximation of integral terms in Section A.5. We then show that these approximations lead to the conservation of tubulin mass in Section A.6. In last Section A.7, we focus on the adaptative time steps that we choose.

A.1. Discretization and unknowns

Time discretization

Let $0 = t_0 < \ldots < t_n < \ldots t_{Nt} = T$ be a discretization of $]0, T[$. We note $\mathrm{d}t_n = t_{n+1} - t_n$ and choose $\mathrm{d}t_n$ to ensure the L^∞ stability of our scheme (see Sect. A.7 for more details).

Age discretization

We introduce the sequence (a_k^n) defined as follow:

$$a_{k+1}^n - a_k^n = \mathrm{d}t_{n-k} := \varepsilon_k^n, \quad with \quad a_0^n = 0$$

and $\varepsilon_{k+1}^{n+1} = \varepsilon_k^n$, $\forall k \geq 1$.

The 1D discretization

We introduce a mesh $\mathcal{T}$ in $[0, x_{\max}]$ consisting of open intervals $K_i =](i-1)h, ih[$, $i = 1, \ldots, N_x$ of the length h. Let $x_i = \left(i - \frac{1}{2}\right)h$ be the center of the cell K_i.

The 2D discretization

Let $\mathcal{M}$ be a mesh of the domain $\{(x, z) \in \mathbb{R}^2$ such that $0 \leq z \leq x \leq x_{\max}\}$. Denote by M_{ij} $i = 1, \ldots, N_x$, $j = 1, \ldots, i$ the elements of the mesh $\mathcal{M}$. The mesh is composed of both triangles (cells M_{ii}, $i = 1, \ldots, N_x$) and squares (cells M_{ij}, $i = 2, \ldots, N_x$, $j = 1, \ldots, i-1$) as shown in Figure A.1. We denote a generic edge of any cell by $\sigma \in \mathcal{E}_M$, where $\mathcal{E}_M$ is the set of all edges of the control volume M and by P_M the center of the cell.
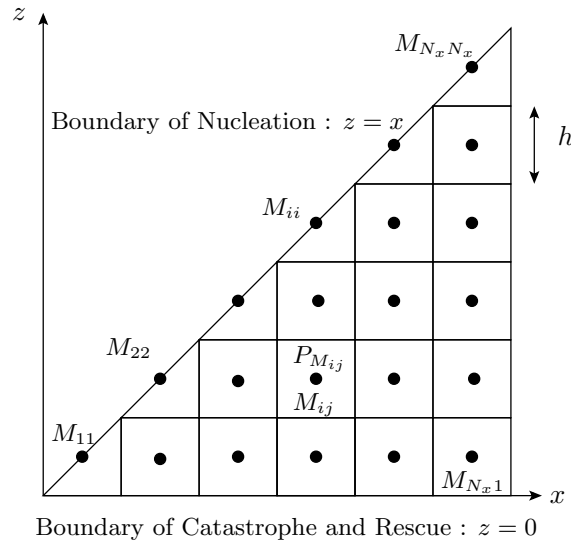
FIGURE A.1. Notations for the mesh $\mathcal{M}$.

Note that we choose $x_{\max}$ sufficiently large so that for $t < T$, the support of the exact solutions $u(t,.)$ and $v(t,.)$ is included in $[0, x_{\max})^2$ and $[0, x_{\max})$ respectively.

Unknowns

The objectif of our numerical scheme is to define sequences $(p^n)_n$, $(q^n)_n$, $(v_i^n)_{n,i}$ and $(u_{k,i,j}^n)_{n,k,i,j}$ in such a way that p^n, q^n, v_i^n and $u_{k,i,j}^n$ approximate respectively the solutions of the continuous model p at time t_n, q at time t_n, v at (t_n, x_i) and u at $(t_n, a_k^n, P_{M_{ij}})$.

A.2. Approximation of ODEs

We approximate equations (2.10) and (2.12) in time using an explicit Euler strategy. In particular, the time evolution of the quantity of free GTP-tubulin p is given by

$$p^{n+1} = p^n - dt_n(\gamma_{\mathrm{pol}}(p^n)I_{u \to p}^n + \kappa q^n - \mathcal{N}(p)), \, p_0 = p(0). \tag{A.1}$$

The discrete equation for the quantity of free GDP tubulin q will be of the form

$$q^{n+1} = q^n + \mathrm{d}t_n(\gamma_{\mathrm{depol}}I_{v \to q}^n - \kappa q^n), \, q_0 = q(0). \tag{A.2}$$

The quantities $I_{u \to p}^n$ and $I_{v \to q}^n$ are approximations of the integral terms $I_{u \to p}$ and $I_{v \to q}$ in equations (2.10) and (2.12) that will be given later.

A.3. Approximation of the PDE for the density $v(t, x)$

We use an Euler explicit scheme in time and an upwind strategy in size x that leads to

$$v_i^{n+1} = v_i^n + \frac{\mathrm{d}t_n \, \gamma_{\mathrm{depol}}}{h}(v_{i+1}^n - v_i^n) + \mathrm{d}t_n(I_{u \to v}^{n,i} - I_{v \to u}^{n,i}). \tag{A.3}$$

Approximations $I_{u \to v}^{n,i}$ and $I_{v \to u}^{n,i}$ for the integral terms $\int_{K_i} I_{v \to u}(t_n, x)$ and $\int_{K_i} I_{u \to v}(t_n, x)$ of catastrophes and rescues will be defined later. The initial condition is given by $v_i^0 = v(0, x_i)$. We assume that $v_{N_x}^n = 0$ for all $0 \le n \le N_t$. This boundary condition make sense while the domain in size is sufficiently large with respect to T.

A.4. Approximation of the PDE for the density $u(t, a, x, z)$

We use an Euler explicit scheme in time and an upwind strategy in size (x, z) and a semi-lagrangian approach in age. Note that in case of constant time steps, this strategy simply leads to an upwind strategy. In case of adaptative time step, this semi-lagragian approach enable us to be more accurate in the frequency estimation for a very low cost.

Let $R_k^n = R(t_n, a_k^n)$ for all n and k. Assume that there exists a Θ^* such that $a_0 < \Theta^* < dt_n$ for all n. We can thus approximate $\Theta(a_k^n)$ given in (2.5) by

$$\Theta_k^n = \begin{cases} 0, & \text{if } k \geq 2, \\ 1/\varepsilon_1^n, & \text{if } k = 1, \end{cases} \tag{A.4}$$

and so $\sum_k \varepsilon_k^n \Theta_k^n = 1$.

The scheme reads for M_{ij}, $i = 2, \ldots, N_x$, $j = 1, \ldots, i-1$, $k = 2, \ldots, n$

$$u_{kij}^{n+1} = u_{k-1ij}^n - \frac{dt_n}{h}\gamma_{\text{pol}}(p^n)(u_{k-1ij}^n - u_{k-1i-1j}^n) - \frac{dt_n}{h}(R_{k-1}^n)^-(u_{k-1ij}^n - u_{k-1ij+1}^n)$$
$$- \frac{dt_n}{h}(R_{k-1}^n)^+(u_{k-1ij}^n - u_{k-1ij-1}^n), \tag{A.5}$$

and for M_{ii}, $i = 1, \ldots, N_x$, $k = 2, \ldots, n$

$$u_{\text{kii}}^{n+1} = u_{k-1ii}^n - \frac{2dt_n}{h}\gamma_{\text{pol}}(p^n)u_{k-1ii}^n - \frac{2dt_n}{h}(R_{k-1}^n)^-u_{k-1ii}^n \tag{A.6}$$

$$+ \frac{2dt_n}{h}(R_{k-1}^n)^+u_{k-1ii-1}^n + \frac{2dt_n}{h}\gamma_{\text{hydro}}(a_{k-1}^n)u_{k-1ii+1}^n. \tag{A.7}$$

with the convention $u_{ki0}^n = 0$, $u_{\text{kii}+1}^n = 0$ for all n, $i = 1, \ldots, N_x$, $k = 2, \ldots, n$. The scheme is endowed by boundary conditions on the "age boundary" $a = 0$

$$u_{1ij}^n = 0, \ n \geq 0, \ i = 1, \ldots, N_x, \ j = 1, \ldots, i, \tag{A.8}$$

on the "catastrophe/rescue boundary" $z = 0$ as $R_1^n > 0$ for all n,

$$R_1^n u_{1i0}^n = \lambda v_i^n \Theta_1^n, \quad \text{for} \quad i = 1 \ldots, N_x, \tag{A.9}$$

and on the "nucleation boundary" $z = x$

$$\gamma_{\text{hydro}}(a_1^n)u_{1ii+1}^n = \mathcal{N}(p^n)\psi(x_i)\Theta_1^n. \tag{A.10}$$

A.5. Approximation of integral terms

Going back to the discrete equations (A.1), (A.2) and (A.3), we provide the approximation of the integral terms by the following expressions

$$I_{u\to p}^n = \sum_{i=1}^{N_x}\sum_{j=1}^{i} h^2 U_{ij}^n, \quad \text{where } U_{ij}^n = \sum_{k=1}^{n}\varepsilon_k^n u_{\text{kij}}^n, \tag{A.11}$$

$$I_{v\to q}^n = \sum_{i=1}^{N_x} hv_i^n - \frac{h}{2}v_1^n, \tag{A.12}$$

$$I_{u\to v}^{n,i} = \sum_{k=1}^{n}\varepsilon_k^n(R_k^n)^- u_{\text{ki}1}^n, \tag{A.13}$$

$$I_{v\to u}^{n,i} = \lambda v_i^n. \tag{A.14}$$

A.6. Conservation of the total tubulin at the discrete level

Let L_u^n be a total amount of tubulin (both α and β tubulin) contained in growing MTs, and L_v^n be a total amount of GDP tubulin contained in shortening MTs. Then

$$L_v^n = h \sum_{i=1}^{N_x} x_i v_i^n, \quad L_u^n = h^2 \sum_{i=1}^{N_x} \sum_{j=1}^{i} x_i U_{ij}^n.$$

Remark A.1. To preserve the total amount of tubulin in the system on a discrete level, approximations of the integral terms $I_{u \to p}$ and $I_{v \to q}$ have been chosen with corrections in the sum of diagonal cells (*i.e.* $i = j$) in (A.11) and for the first segment (*i.e.* $i = 1$) in (A.12).

Total amount of tubulin in the system is written as

$$\chi_n = L_u^n + L_v^n + p^n + q^n,$$

We state the theorem for the conservation law of tubulin mass on a discrete level.

Theorem A.2. *There exists N_0 such that $\chi_n = \chi_0$ for all $n \leq N_0$.*

Note that if we choose $x_{\max}$ sufficiently large with respect to T, then $n_0 = N_t$.

Before the proof of the Theorem 1, let us formulate several auxiliary lemmas. The following lemma is given to serve for convenience in writing.

Lemma A.3. *The discrete equation* (A.5) *for the square cells M_{ij}, $i = 2, \ldots, N_x$, $j = 1, \ldots, i-1$, $k = 1, \ldots, n$ can be rewritten for U_{ij}^{n+1} given in* (A.11) *in the form*

$$U_{ij}^{n+1} = U_{ij}^n - \frac{dt_n}{h} \gamma_{\text{pol}}(p^n)(U_{ij}^n - U_{i-1j}^n) - \frac{dt_n}{h} \sum_{k=1}^{n} \varepsilon_k^n (R_k^n)^- (u_{\text{k}ij}^n - u_{\text{k}ij+1}^n)$$

$$- \frac{dt_n}{h} \sum_{k=1}^{n} \varepsilon_k^n (R_k^n)^+ (u_{\text{k}ij}^n - u_{\text{k}ij-1}^n).. \tag{A.15}$$

The discrete equation (A.7) *for the triangular cells M_{ii}, $i = 1, \ldots, N_x$, $k = 1, \ldots, n$ can be rewritten for U_{ii}^{n+1} in the form*

$$U_{ii}^{n+1} = U_{ii}^n - \frac{2dt_n}{h} \gamma_{\text{pol}}(p^n) U_{ii}^n - \frac{2dt_n}{h} \sum_{k=1}^{n} \varepsilon_k^n (R_k^n)^- u_{\text{k}ii}^n + \frac{2dt_n}{h} \sum_{k=1}^{n} \varepsilon_k^n (R_k^n)^+ u_{\text{k}ii-1}^n$$

$$+ \frac{2dt_n}{h} \varepsilon_1^n \gamma_{\text{hydro}}(dt_n) u_{1ii+1}^n. \tag{A.16}$$

Lemma A.4. *The difference between tubulin mass in growing MTs at the $(n+1)$th and nth time steps is given by the right-hand side of*

$$L_u^{n+1} - L_u^n = \Delta_{u-} + \Delta_{u+} + \Delta_{u,\text{pol}} + \Delta_{u,\text{nucl}}, \tag{A.17}$$

where the following notations are used

$$\Delta_{u-} = -h dt_n \sum_{i=1}^{N_x} x_i I_{u \to v}^{n,i}, \quad \Delta_{u+} = h dt_n \lambda \sum_{i=1}^{N_x} x_i v_i^n,$$

$$\Delta_{u,\text{pol}} = dt_n \gamma_{\text{pol}}(p^n) I_{u \to p}^n, \quad \Delta_{u,\text{nucl}} = dt_n \mathcal{N}(p^n).$$

Proof. We group terms of the difference $L_u^{n+1} - L_u^n$ in the following way and reduce them to Δ_{u-}, Δ_{u+}, $\Delta_{u,\text{pol}}$.

The expression for the tubulin mass contained in MTs that undergo catastrophe is given on the left side of the following expression and further it is transformed to Δ_{u-}

$$-h\mathrm{d}t_n \sum_{i=1}^{N_x} \sum_{j=1}^{i} \sum_{k=2}^{n} \varepsilon_k^n (R_k^n)^- x_i (u_{kij}^n - u_{kij+1}^n) = -h\mathrm{d}t_n \sum_{k=2}^{n} \varepsilon_k^n (R_k^n)^- \sum_{i=1}^{N_x} \sum_{j=1}^{i} x_i (u_{kij}^n - u_{kij+1}^n)$$

$$= -h\mathrm{d}t_n \sum_{k=2}^{n} \varepsilon_k^n (R_k^n)^- \sum_{i=1}^{N_x} x_i u_{ki1}^n = -h\mathrm{d}t_n \sum_{i=1}^{N_x} x_i \sum_{k=2}^{n} \varepsilon_k^n (R_k^n)^- u_{ki1}^n$$

$$= -h\mathrm{d}t_n \sum_{i=1}^{N_x} x_i I_{u\to v}^{n,i} = \Delta_{u-},$$

The expression for the quantity of tubulin polymerized in MTs undergoing rescue has the following form that we reduce to Δ_{u+}

$$-h\mathrm{d}t_n \left(\sum_{i=2}^{N_x} \sum_{j=1}^{i-1} x_i \sum_{k=1}^{n} \varepsilon_k^n (R_k^n)^+ (u_{kij}^n - u_{kij-1}^n) - \sum_{i=1}^{N_x} x_i \sum_{k=1}^{n} \varepsilon_k^n (R_k^n)^+ u_{kii-1}^n \right)$$

$$= -h\mathrm{d}t_n \sum_{k=1}^{n} \varepsilon_k^n (R_k^n)^+ \left(\sum_{i=2}^{N_x} \sum_{j=1}^{i-1} x_i (u_{kij}^n - u_{kij-1}^n) - \sum_{i=1}^{N_x} x_i u_{kii-1}^n \right)$$

$$= -h\mathrm{d}t_n \sum_{k=1}^{n} \varepsilon_k^n (R_k^n)^+ \left(\sum_{i=2}^{N_x} x_i (u_{kii-1}^n - u_{ki0}^n) - \sum_{i=1}^{N_x} x_i u_{kii-1}^n \right)$$

$$= h\mathrm{d}t_n \sum_{k=1}^{n} \varepsilon_k^n (R_k^n)^+ \sum_{i=1}^{N_x} x_i u_{ki0}^n = h\mathrm{d}t_n \varepsilon_1^n (R_1^n)^+ \sum_{i=1}^{N_x} x_i u_{1i0}^n$$

$$= h\mathrm{d}t_n \sum_{i=1}^{N_x} x_i \lambda v_i^n = \Delta_{u+}.$$

Taking advantage of Lemma 2, we calculate the tubulin contained in MTs in polymerization state using the equations (A.15) and (A.16)

$$-h\mathrm{d}t_n \gamma_{\text{pol}}(p^n) \left(\sum_{i=2}^{N_x} \sum_{j=1}^{i-1} x_i (U_{ij}^n - U_{i-1j}^n) + \sum_{i=1}^{N_x} x_i U_{ii}^n \right)$$

$$= -h\mathrm{d}t_n \gamma_{\text{pol}}(p^n) \left(\sum_{j=1}^{N_x-1} \sum_{i=j+1}^{N_x} x_i U_{ij}^n - \sum_{j=1}^{N_x-1} \sum_{i=j}^{N_x-1} x_{i+1} U_{ij}^n + \sum_{i=1}^{N_x} x_i U_{ii}^n \right)$$

We sum the first and the last terms and add to the second term $\sum_{j=1}^{N_x} x_{N_x+1} U_{N_x j}^n$ that we imply to be zero. Note that due to the finite propagation speed of the transport equation $\exists N_0 : \forall n \leq N_0, \ U_{N_x j}^n = 0, \ \forall j$. Recalling that $x_{i+1} - x_i = h$ we get

$$-h\mathrm{d}t_n \gamma_{\text{pol}}(p^n) \left(\sum_{i=1}^{N_x} \sum_{i=j}^{N_x} x_i U_{ij}^n - \sum_{j=1}^{N_x} \sum_{i=j}^{N_x} x_{i+1} U_{ij}^n \right) = h^2 \mathrm{d}t_n \gamma_{\text{pol}}(p^n) \sum_{i=1}^{N_x} \sum_{j=1}^{i} U_{ij}^n$$

$$= \mathrm{d}t_n \gamma_{\text{pol}}(p^n) I_{u\to p}^n = \Delta_{u,\text{pol}},$$

The expression of the tubulin mass polymerized in nucleated MTs has the following form and reduced to $\Delta_{u,\mathrm{nucl}}$

$$\frac{h^2}{2}\sum_{i=1}^{N_x}\varepsilon_1^n x_i\frac{2\mathrm{d}t_n}{h}\gamma_{\mathrm{hydro}}(\mathrm{d}t_n)u_{1i\ i+1}^n = \mathrm{d}t_n\,h\mathcal{N}(p^n)\sum_{i=1}^{N_x}x_i\psi_i = \mathrm{d}t_n\,\mathcal{N}(p^n) = \Delta_{u,\mathrm{nucl}}.$$

The lemma is proved. $\qquad\square$

Lemma A.5. *The difference between tubulin mass contained in shortening MTs at the nth and $(n+1)$th time steps is given by*

$$L_v^{n+1} - L_v^n = \Delta_{v,\gamma_{\mathrm{depol}}} + \Delta_{v,u+} + \Delta_{v,u-}. \tag{A.18}$$

where

$$\Delta_{v,\gamma_{\mathrm{depol}}} = -\mathrm{d}t_n\gamma_{\mathrm{depol}}I_{v\to q}^n, \quad \Delta_{v,u+} = -h\mathrm{d}t_n\lambda\sum_{i=1}^{N_x}x_i v_i^n,$$

$$\Delta_{v,u-} = h\,\mathrm{d}t_n\sum_{i=1}^{N_x}x_i I_{u\to v}^{n,i}.$$

Proof. We write out each term of the difference $L_v^{n+1} - L_v^n$ and transform them to $\Delta_{v,\gamma_{\mathrm{depol}}}$, $\Delta_{v,u+}$, $\Delta_{v,w-}$, and $\Delta_{v,u-}$.

The expression for the quantity of tubulin in depolymerizing MTs can be reduced in the following way

$$\mathrm{d}t_n\gamma_{\mathrm{depol}}\left(\sum_{i=2}^{N_x+1}v_i^n x_{i-1} - \sum_{i=1}^{N_x}v_i^n x_i\right) = \mathrm{d}t_n\gamma_{\mathrm{depol}}\left(\sum_{i=2}^{N_x}v_i^n(x_{i-1} - x_i)\right.$$

$$+v_{N_x+1}^n x_{N_x} - v_1^n x_1\Big) = \mathrm{d}t_n\gamma_{\mathrm{depol}}\left(-h\sum_{i=2}^{N_x}v_i^n + v_{N_x+1}^n x_{N_x} - v_1^n x_1\right)$$

$$= \mathrm{d}t_n\gamma_{\mathrm{depol}}\left(-h\sum_{i=1}^{N_x}v_i^n + \frac{h}{2}v_1^n\right) = -\mathrm{d}t_n\gamma_{\mathrm{depol}}I_{v\to q}^n = \Delta_{v,\gamma_{\mathrm{depol}}}.$$

The expression for the tubulin mass contained in MTs undergoing rescue has the following form

$$-h\mathrm{d}t_n\lambda\sum_{i=1}^{N_x}x_i v_i^n = \Delta_{v,u+},$$

The quantity of the tubulin contained in MTs undergoing catastrophe is calculated as the following

$$h\,\mathrm{d}t_n\sum_{k=1}^{n}\varepsilon_k^n(R_k^n)^- \sum_{i=1}^{N_x}x_i u_{ki1}^n = h\,\mathrm{d}t_n\sum_{i=1}^{N_x}x_i I_{u\to v}^{n,i} = \Delta_{v,u-}.$$

The lemma is proved. $\qquad\square$

Proof of the theorem 1. We rewrite the equations for free GTP-tubulin p^{n+1} and for free GDP-tubulin q^{n+1} in following way

$$p^{n+1} - p^n = \Delta_{p,u} + \Delta_{p,q} + \Delta_{p,\mathrm{nucl}}, \tag{A.19}$$

where $\Delta_{p,u} = -dt_n\gamma_{\mathrm{pol}}(p^n)I_{u\to p}^n$, $\Delta_{p,q} = \mathrm{d}t_n\kappa q^n$, $\Delta_{p,\mathrm{nucl}} = -\mathrm{d}t_n\mathcal{N}(p^n)$,

$$q^{n+1} - q^n = \Delta_{q,\gamma_{\mathrm{depol}}} + \Delta_{q,p}, \tag{A.20}$$

where $\Delta_{q,\gamma_{\text{depol}}} = \mathrm{d}t_n \gamma_{\text{depol}} I^n_{v \to q}$, $\Delta_{q,p} = -\mathrm{d}t_n \kappa q^n$.

Now, we consider the difference $\chi_{n+1} - \chi_n$ that is the difference between the total tubulin mass of the system at the $(n+1)$th and nth time instant and take advantage of the terms from the right sides of equations (A.17)–(A.20). Gathering them in the following way,

$$\chi_{n+1} - \chi_n = (\Delta_{u,nucl} + \Delta_{p,\text{nucl}}) + (\Delta_{u-} + \Delta_{v,u-}) + (\Delta_{u,\text{pol}} + \Delta_{p,u})$$
$$+ (\Delta_{v,\gamma_{\text{depol}}} + \Delta_{q,\gamma_{\text{depol}}}) + (\Delta_{u+} + \Delta_{v,u+}) + (\Delta_{p,q} + \Delta_{q,p}),$$

where the terms are zero in each parenthesis. Therefore, we proved that the total tubulin mass in the system on a discrete level remains constant over time. □

A.7. Time step

The computations are carried out with adaptive time step that is a maximal time step for which the scheme is L^∞−stable. In particular, we have

$$\mathrm{d}t_n \leq \min \left(\frac{h}{\gamma_{\text{pol}}(p^n) + \max\limits_{2 \leq k \leq n+1} |R^n_{k-1}|}, \; \frac{h}{2(\gamma_{\text{pol}}(p^n) + \max\limits_{2 \leq k \leq n+1} (R^n_{k-1})^-)}, \right.$$
$$\left. \frac{h}{(\gamma_{\text{depol}} + \lambda)}, \frac{p^n}{\mathcal{N}(p^n) + \gamma_{\text{pol}}(p^n) I^n_{u \to p}}, 1/\kappa \right) \tag{A.21}$$

References

[1] A. Akhmanova and M. Steinmetz, Microtubule end binding: Ebs sense the guanine nucleotide state. *Curr. Biol.* **21** (2011) R283–5.

[2] T. Antal, P. Krapivsky, S. Redner, M. Mailman and B. Chakraborty, Dynamics of an idealized model of microtubule growth and catastrophe. *Phys. Rev. E Stat. Nonlin. Soft. Matter Phys.* **76** (2007) 907.

[3] I. Arnal and R. Wade, How does taxol stabilize microtubules? *Curr. Biol.* **5** (1995) 900–908.

[4] H. Bowne-Anderson, M. Zanic, M. Kauer and J. Howard, Microtubule dynamic instability: a new model with coupled gtp hydrolysis and multistep catastrophe. *Bioessays* **35** (2013) 579.

[5] G. Brouhard and D. Sept, Microtubules: sizing up the gtp cap. *Curr. Biol.* **22** (2012) R802–3.

[6] G. Buxton, S. Siedlak, G. Perry and S. Ma, Mathematical modeling of microtubule dynamics: insights into physiology and disease. *Prog. Neurobiol.* **92** (2010) 478–483.

[7] Y. Chen and T. Hill, Monte Carlo study of the GTP cap in a five-start helix model of a microtubule. *Proc. Natl. Acad. Sci. USA* **82** (1985) 1131–1135.

[8] C. Coombes, A. Yamamoto, M. Kenzie, D. Odde and M. Gardner, Evolving tip structures can explain age-dependent microtubule catastrophe. *Curr. Biol.* **23** (2013) 1342–1348.

[9] A. Desai and T. Mitchison, Microtubule polymerization dynamics. *Annu. Rev. Cell. Dev. Biol.* **13** (1997) 83–117.

[10] J. Díaz, J. Andreu and J. Jiménez-Barbero, *The Interaction of Microtubules with Stabilizers Characterized at Biochemical and Structural Levels.* In Vol. 286 of Tubulin-Binding Agents (2008).

[11] M. Dogterom and S. Leibler, Physical aspects of the growth and regulation of microtubule structures. *Phys. Rev. Lett.* **70** (1993) 1347–1350.

[12] H. Flyvbjerg, T. Holy and S. Leibler, Stochastic dynamics of microtubules: a model for caps and catastrophes. *Phys. Rev. Lett.* **73** (1994) 2372–2375.

[13] N. Galjart, Plus-end-tracking proteins and their review interactions at microtubule ends. *Cur. Biol.* **20** (2010) R528–R537.

[14] M. Gardner, M. Zanic, C. Gell, V. Bormuth and J. Howard, Depolymerizing kinesins kip3 and mcak shape cellular microtubule architecture by differential control of catastrophe. *Cell* **147** (2011) 1092–1103.

[15] F. Hallett, Rapid estimation of length distributions of microtubule preparations by quasi-elastic light scattering. *Biopolymers* **24** (1985) 2403–2415.

[16] P. Hinow, V. Rezania, M. Lopus, M. Jordan and J. Tuszyński, Modeling the effects of drug binding on the dynamic instability of microtubules. *Phys. Biol.* **8** (2011) 056004.

[17] P. Hinow, V. Rezania and J. Tuszyński, Continuous model for microtubule dynamics with catastrophe, rescue, and nucleation processes. *Phys. Rev. E Stat. Nonlin. Soft. Matter Phys.* **80** (2009) 031904.

[18] S. Honoré and D. Braguer, Investigating microtubule dynamic instability using microtubule-targeting agents. *Methods Mol. Biol.* **777** (2011) 245–260.

[19] S. Honoré, E. Pasquier and D. Braguer, Understanding microtubule dynamics for improved cancer therapy. *Cell. Mol. Life Sci.* **62** (2005) 3039–3056.

[20] A. Janulevicius, J. van Pelt and van A. Ooyen, Compartment volume influences microtubule dynamic instability: a model study. *Biophys. J.* **90** (2006) 788–98.

[21] V. Jemseena and M. Gopalakrishnan, Effects of aging in catastrophe on the steady state and dynamics of a microtubule population. *Phys. Rev. E Stat. Nonlin. Soft. Matter Phys.* **91** (2015) 052704.

[22] X. Ji and X. Feng, Mechanochemical modeling of dynamic microtubule growth involving sheet-to-tube transition. *PLoS One* **6** (2011) e29049.

[23] M. Le Grand, A. Rovini, V. Bourgarel-Rey, S. Honoré, S. Bastonero, D. Braguer and M. Carre, Ros-mediated eb1 phosphorylation through akt/gsk3β pathway: implication in cancer cell response to microtubule-targeting agents. *Oncotarget* **5** (2014) 3408–3423.

[24] H. Lodish, A. Berk, S.L. Zipursky, P. Matsudaira, D. Baltimore and J. Darnell, Molecular cell biology, 4th edn. W.H. Freeman and Company, New York (2000).

[25] Q. Lu and R. Luduena, In vitro analysis of microtubule assembly of isotypically pure tubulin dimers. intrinsic differences in the assembly properties of alpha beta ii, alpha beta iii, and alpha beta iv tubulin dimers in the absence of microtubule-associated proteins. *J. Biol. Chem.* **269** (1994) 2041–2047.

[26] S. Martin, M. Schilstra and P. Bayley, Dynamic instability of microtubules: Monte carlo simulation and application to different types of microtubule lattice. *Biophys. J.* **65** (1993) 578–596.

[27] S. Maurer, F. Fourniol, G. Bohner, C. Moores and T. Surrey, Ebs recognize a nucleotide-dependent structural cap at growing microtubule ends. *Cell* **149** (2012) 371–382.

[28] M. Mirigian, K. Mukherjee, S.L. Bane and D.L. Sackett, Measurement of In vitro Microtubule polymerization by turbidity and fluorescence. *Meth. Cell. Biol.* **115** (2013) 215–228.

[29] T. Mitchison and M. Kirschner, Dynamic instability of microtubule growth. *Nature* **312** (1984) 237–242.

[30] R. Mohan, E. Katrukha, H. Doodhi, I. Smal, E. Meijering, L. Kapitein, M. Steinmetz and A. Akhmanova, End-binding proteins sensitize microtubules to the action of microtubule-targeting agents. *Proc. Natl. Acad. Sci. USA* **110** (2013) 8900–8905.

[31] S. Montenegro Gouveia, K. Leslie, L. Kapitein, R. Buey, I. Grigoriev, M. Wagenbach, I. Smal, E. Meijering, C. Hoogenraad, L. Wordeman, M. Steinmetz and A. Akhmanova, In vitro reconstitution of the functional interplay between mcak and eb3 at microtubule plus ends. *Curr. Biol.* **20** (2010) 1717–1722.

[32] N. Müller and J. Kierfeld, Effects of microtubule mechanics on hydrolysis and catastrophes. *Phys. Biol.* **11** (2014) 046001.

[33] R. Padinhateeri, A. Kolomeisky and D. Lacoste, Random hydrolysis controls the dynamic instability of microtubules. *Biophys. J.* **102** (2012) 1274–1283.

[34] A. Pagano, S. Honoré, R. Mohan, R. Berges, A. Akhmanova and D. Braguer, Epothilone b inhibits migration of glioblastoma cells by inducing microtubule catastrophes and affecting eb1 accumulation at microtubule plus ends. *Biochem. Pharmacol.* **84** (2012) 432–443.

[35] D. Seetapun, B. Castle, A. McIntyre, P. Tran and D. Odde, Estimating the microtubule gtp cap size in vivo. *Curr. Biol.* **22** (2012) 1681–1687.

[36] V. VanBuren, L. Cassimeris and D. Odde, Mechanochemical model of microtubule structure and self-assembly kinetics. *Biophys. J.* **89** (2005) 2911–2926.

[37] R. Walker, E. O'Brien, N. Pryer, M. Soboeiro, W. Voter, Erickson and H. E. Salmon, Dynamic instability of individual microtubules analyzed by video light microscopy: Rate constants and transition frequencies. *J. Cell. Biol.* **107** (1988) 1437–1448.

[38] P. Zakharov, N. Gudimchuk, V. Voevodin, A. Tikhonravov, F. Ataullakhanov and E. Grishchuk, Molecular and mechanical causes of microtubule catastrophe and aging. *Biophys. J.* **109** (2015) 2574–2591.